Investigation of Three-Dimensional Stress Fields and Slip Systems for fcc Single-Crystal Superalloy Notched Specimens

Nagaraj K. Arakere
Associate Professor

Shadab Siddiqui
Graduate Student

Mechanical and Aerospace Engineering,
University of Florida,
Gainesville, FL 32611-6300

Shannon Magnan
Lieutenant Junior Grade,
U.S. Navy Reserve

Fereshteh Ebrahimi
Professor

Luis E. Forero
Graduate Student

Materials Science and Engineering,
University of Florida,
Gainesville, FL 32611-6300

Metals and their alloys, except for a few intermetallics, are inherently ductile, i.e., plastic deformation precedes fracture in these materials. Therefore, resistance to fracture is directly related to the development of the plastic zone at the crack tip. Recent studies indicate that the fracture toughness of single crystals depends on the crystallographic orientation of the notch as well as the loading direction. In general, the dependence of crack propagation resistance on crystallographic orientation arises from the anisotropy of (i) elastic constants, (ii) plastic deformation (or slip), and (iii) the weakest fracture planes (e.g., cleavage planes). Because of the triaxial stress state at the notch tips, many slip systems that otherwise would not be activated during uniaxial testing become operational. The plastic zone formation in single crystals has been tackled theoretically by Rice and his co-workers [Rice, J. R., 1987, Mech. Mater. ***6****, pp. 317–335; Rice, J. R., and Saeedvafa, M., 1987, J. Mech. Phys. Solids* ***36****, pp. 189–214; Saeedvafa, M., and Rice, J. R., 1988; ibid.,* ***37****, pp. 673–691; Rice, J. R., Hawk, D. E., Asaro, R. J., 1990, Int. J. Fract.* ***42****, pp. 301–321; Saeedvafa, M., and Rice, J. R., 1992, Modell. Simul. Mater. Sci. Eng.* **1**, *pp. 53–71] and only limited experimental work has been conducted in this area. The study of the stresses and strains in the vicinity of a fcc single-crystal notch tip is of relatively recent origin. We present experimental and numerical investigation of three-dimensional (3D) stress fields and evolution of slip sector boundaries near notches in fcc single-crystal PWA1480 tension test specimens and demonstrate that a 3D linear elastic finite element model, which includes the effect of material anisotropy, is shown to predict active slip planes and sectors accurately. The slip sector boundaries are shown to have complex curved shapes with several slip systems active simultaneously near the notch. Results are presented for surface and mid-plane of the specimens. The results demonstrate that accounting for 3D elastic anisotropy is very important for accurate prediction of slip activation near fcc single-crystal notches loaded in tension. Results from the study will help establish guidelines for fatigue damage near single-crystal notches.*
[DOI: 10.1115/1.1850939]

Introduction

Turbine blades and vanes in high-performance aircraft and rocket engines are increasingly being made of single-crystal nickel superalloys. Single-crystal nickel-base superalloys were developed to provide superior creep, stress rupture, melt resistance, and thermomechanical fatigue capabilities over polycrystalline alloys previously used in the production of turbine blades and vanes. Currently these single-crystal nickel-base turbine blade superalloys are widely used in aircraft and rocket engine applications and are also being used in the NASA SSME alternate fuel turbopump. These alloys play an important role in commercial, military, and space propulsion systems. Single-crystal materials differ significantly from polycrystalline alloys in that they have highly orthotropic properties, making the position of the crystal lattice relative to the part geometry a significant factor in the overall analysis. Turbine blades and vanes, used in aircraft and rocket engines, are typically the most demanding structural applications for high-temperature materials due to the combination of high operating temperature, corrosive environment, high monotonic and cyclic stresses, long expected component lifetimes, and the enormous consequence of structural failure. Hence failures of blade components account for 40% of all turbine engine component failures attributable to HCF. Estimation of blade fatigue life, therefore, represents a very important aspect of durability assessment.

Metals and their alloys, except for a few intermetallics, are inherently ductile, i.e., plastic deformation precedes fracture in these materials. Therefore, resistance to fracture is directly related to the development of the plastic zone at the crack tip. Recent studies indicate that the fracture toughness of single crystals depends on the crystallographic orientation of the notch (here referred to as the secondary orientation) as well as the loading direction (here referred to as primary orientation) [1–9]. In general, the dependence of crack propagation resistance on crystallographic orientation arises from the anisotropy of (i) elastic constants, (ii) plastic deformation (or slip), and (iii) the weakest fracture planes (e.g., cleavage planes). As far as crack initiation and propagation in metallic alloys are concerned, the effect of crystallographic orientation on the development of the plastic zone in the vicinity of a crack tip is of significant importance. In polycrystal-

Contributed by the International Gas Turbine Institute (IGTI) of THE AMERICAN SOCIETY OF MECHANICAL ENGINEERS for publication in the ASME JOURNAL OF ENGINEERING FOR GAS TURBINES AND POWER. Paper presented at the International Gas Turbine and Aeroengine Congress and Exhibition, Vienna, Austria, June 13–17, 2004, Paper No. 2004-GT-53938. Manuscript received by IGTI, October 1, 2003; final revision, March 1, 2004. IGTI Review Chair: A. J. Strazisar.

line metals, although the far field stresses are controlled by their isotropic properties, the behavior at the crack tip is partially governed by the crystal anisotropy.

Many groups have used dislocation theory to study the initiation of plasticity at crack tips and notches, in semi-brittle materials [10–15], however, only limited work has been reported on the development of plastic zones at meso- and macroscopic levels in notched ductile single crystals. Because of the triaxial stress state at the notch tips, many slip systems that otherwise would not be activated during uniaxial testing become operational. The plastic zone formation in single crystals has been tackled theoretically by Rice and his co-workers [16–20], and only limited experimental work has been conducted in this area [21–25].

The study of the stresses and strains in the vicinity of a fcc single-crystal notch tip is of relatively recent origin; despite the analytical and experimental investigations by researchers [16,21–25], a single-crystal model that incorporates 3D elastic anisotropy and near-notch plasticity effects, necessary to accurately predict evolution of slip sectors in 3D stress fields, is far from complete. This paper presents an experimental and numerical investigation of 3D stress fields and evolution of slip sector boundaries near notches in fcc single-crystal tension test specimens and demonstrates that a 3D linear elastic finite element model, which includes the effect of material anisotropy, is shown to predict active slip planes and sectors accurately. This is a first step toward a comprehensive analysis of the evolution of the plastic zone in notches with triaxial stress fields in single-crystal superalloys. We are developing constitutive relations for modeling crystal plasticity in 3D stress fields, to evaluate both monotonic and cyclic plastic stresses and strains, toward evaluating fatigue life in single-crystal superalloy turbine blades. A rate-dependent constitutive model is being developed [26] that is capable of modeling large deformation and large strains. This model enables unique determination of slip rates on each slip system even when many potential slip systems are included in the model, thus, enabling simulation of multiple slip.

Review of Two-Dimensional Plastic Analysis of Notched Single Crystals

Rice [16] provided the foundation for much recent and current work in the area of crack/notch tip stress and strain analysis by examining the mechanics of both fcc and bcc notched specimens loaded in tension. Rice constructs the plastic field at the crack tip based on plane strain [two-dimensional (2D)] isotropic assumptions, and the results represent a continuous solution in terms of the radial and angular displacement from the tip, where the state of stress is constant within each sector. A perfectly plastic stress field is assumed, and therefore the boundaries are defined as the radial lines where a discontinuity occurs at specific angles where the slip shifts from one system to another. The solution does not distinguish between the two orientations' sector boundaries or between fcc or bcc crystal structure. Both crystal orientations and structures predict boundaries at 55, 90, and 125 deg. Rice notes the weakness of this attribute, based on contradictory experimental studies, which is tied to the rotation of the crystal lattice. He acknowledges the simplification of the plane strain assumption and encourages incorporating anisotropy, strain hardening, and 3D effects into future models.

Shield [21] conducted several tests of notched four-point bending single-crystal copper specimens to correlate Rice's analytical models with his experimental observations. Moiré interferometry analysis was used to determine the strain fields and sectors. Shield's results from the low load levels show similarities to Rice's model, but do not correlate to Rice's model at high plastic strains. The strains do not maintain the same order in their relative level of activity in different sectors. This changing slip activity (with load level) contradicts the constant sector boundaries predicted using 2D isotropic assumptions. Shield's experimental results, and their dissimilarity to Rice's analysis, again highlight the need for a more accurate predictive model.

Crone and Shield [23] continued experimental studies of notch tip deformation in two different orientations of single-crystal copper and copper-beryllium tensile specimens. Slip sector boundaries are determined experimentally, again using Moiré interferometry. The visible slip patterns determine slip activity, but as the authors note, a lack of visible slip does not rule out any activity. Slip systems may be activated internally, rather than at the surface, or may show varying patterns on the surface as deformation continues. They compared their experimental results to Rice's analytical solution, as well as numerical finite element analysis (FEA) solutions by Mohan et al. [27] and Cuitino and Ortiz [28]. Both numerical models are based on the plane strain assumption, although Cuitino and Ortiz later conclude the problem cannot truly be plane strain due to large strain differences internally and at the surface. Even with the plane strain assumption, the numerical and analytical models do not match; all three differ from the experimental results. The experimental results are somewhat ambiguous due to the ''annulus of validity,'' where Crone and Shield take their measurements. This annulus, following Shield and Kim [25] corresponds to the radial area from 350 to 750 μm from the notch tip. The notch width is between 100 and 200 μm, making the notch radius between 50 and 100 μm. Therefore the annulus and the region where the sectors are measured is anywhere from 3.5 to 7.0 and 7.5 to 15.0 times the notch radius from the tip. These distances would place the sectors well out of the range of any elastic deformation and clearly can only be used where extreme plastic deformation exists. However, Crone and Shield preserve this annulus to avoid material too close to the notch tip. They note that observed slip activity begins in a single sector; as deformation proceeds, more slip lines become visible in the same sector at further radial distances from the notch. They also clearly observe horizontal slip traces directly ahead of the notch, however, they discount their observations and label the slip as ''elastic'' in order to compare their solution to other perfectly plastic sharp crack solutions. Citing Saeedvafa and Rice [18] they further explain these traces as a function of hardening and not plastic deformation, but they do not make such accounts for the other sectors. Contrary to the equivalent sectors predicted by Rice, Crone and Shield's observed sectors show a marked difference with orientation, varying in both specific boundary angles and in the number of sectors. The plane strain FEA results on a central plane of the model appeared to correspond more closely to the experimental results. Crone and Shield assert this agreement to the central plane FEA results, which suggests that plane strain is accurate for specific locations.

Schulson and Xu [22] examined the state of stress at a notch tip for single crystal Ni_3Al, the γ' component of single-crystal superalloys, using three-point bending specimens. An analytical model based on elastic isotropic assumptions was used and calculated stress field around the notch based on the equations for a sharp notch. Two solutions based on plane stress and plane strain assumptions were evaluated. They note, however, that since the notch causes a triaxial state of stress, both these assumptions and ignoring anisotropy are approximations. Experimental results after significant plastic deformation reveal results that deviate from those predicted by either plane stress or plane strain, but are closer to the plane stress assumption.

Elastic Anisotropy in fcc Single Crystals

The generalized Hooke's law for a homogeneous anisotropic body in Cartesian coordinates (x, y, z with origin at point O) is given by Eq. (1) [29]

$$\{\boldsymbol{\varepsilon}\}=\lfloor \mathbf{a}_{ij}\rfloor\{\boldsymbol{\sigma}\} \tag{1}$$

$[\mathbf{a}_{ij}]$ is the matrix of 36 elastic coefficients, of which only 21 are independent, since $[\mathbf{a}_{ij}]=[\mathbf{a}_{ji}]$. The elastic properties of FCC

Table 1 Slip plane and slip direction for the 12 primary octahedral slip systems [30]

Slip system	Slip plane ⟨110⟩{111}	Slip direction
1	(111)	$[10\bar{1}]$
2	(111)	$[0\bar{1}1]$
3	(111)	$[1\bar{1}0]$
4	$(\bar{1}1\bar{1})$	$[10\bar{1}]$
5	$(\bar{1}1\bar{1})$	$[110]$
6	$(\bar{1}1\bar{1})$	$[011]$
7	$(1\bar{1}\bar{1})$	$[110]$
8	$(1\bar{1}\bar{1})$	$[0\bar{1}1]$
9	$(1\bar{1}\bar{1})$	$[101]$
10	$(\bar{1}\bar{1}1)$	$[011]$
11	$(\bar{1}\bar{1}1)$	$[101]$
12	$(\bar{1}\bar{1}1)$	$[1\bar{1}0]$

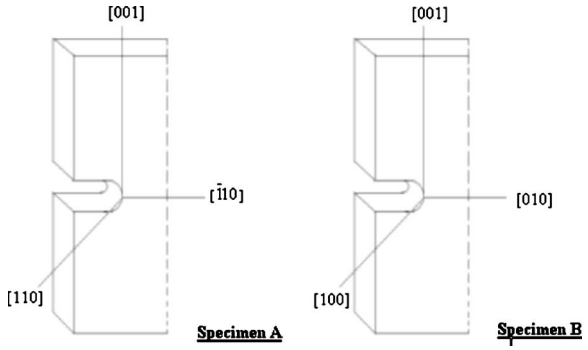

Fig. 1 Finite element analysis, specimens, and orientations [32]

crystals exhibit cubic symmetry, also described as cubic syngony. The elastic properties of materials with cubic symmetry can be described with three independent constants designated as the elastic modulus, shear modulus, and Poisson ratio [29], and hence $[\mathbf{a}_{ij}]$ can be expressed as shown in Eq. (2), in the material coordinate system (fcc crystal axes are parallel to x, y, and z coordinate axes). In contrast to the fcc single-crystal material, an isotropic material can only have two independent elastic constants

$$[\mathbf{a}_{ij}]=\begin{bmatrix} a_{11} & a_{12} & a_{12} & 0 & 0 & 0 \\ a_{12} & a_{11} & a_{12} & 0 & 0 & 0 \\ a_{12} & a_{12} & a_{11} & 0 & 0 & 0 \\ 0 & 0 & 0 & a_{44} & 0 & 0 \\ 0 & 0 & 0 & 0 & a_{44} & 0 \\ 0 & 0 & 0 & 0 & 0 & a_{44} \end{bmatrix} \tag{2}$$

$$a_{11}=\frac{1}{E_{xx}}, \quad a_{44}=\frac{1}{G_{yz}}, \quad a_{12}=-\frac{\nu_{yx}}{E_{xx}}=-\frac{\nu_{xy}}{E_{yy}}$$

The elastic constants in the generalized Hooke's law of an anisotropic body $[\mathbf{a}_{ij}]$ vary with the direction of the coordinate axes. For orientations other than the (x,y,z) axes, the $[\mathbf{a}_{ij}]$ matrix varies with the crystal orientation. In the case of an isotropic body the constants are *invariant* in any orthogonal coordinate system. Consider a Cartesian coordinate system (x',y',z') that has rotated about the origin O of (x,y,z). The elastic constant matrix $[\mathbf{a}'_{ij}]$ in the (x',y',z') coordinate system that relates $\{\boldsymbol{\varepsilon}'\}$ and $\{\boldsymbol{\sigma}'\}$ $[\{\boldsymbol{\varepsilon}'\}=[\mathbf{a}'_{ij}]\{\boldsymbol{\sigma}'\}]$ is given by the following transformation [29]:

$$[\mathbf{a}'_{ij}]=[\mathbf{Q}]^T[\mathbf{a}_{ij}][\mathbf{Q}]=\sum_{m=1}^{6}\sum_{n=1}^{6} a_{mn}Q_{mi}Q_{nj}, \quad (i,j=1,2,\ldots,6) \tag{3}$$

The transformation matrix $[Q]$ is a 6×6 matrix that is a function of the direction cosines between the (x,y,z) and (x',y',z') coordinate axes. Knowing the state of stress at a given location, in the material coordinate system (x,y,z), the resolved shear stresses (RSS) on the 12 primary octahedral slip systems, denoted by τ^1, $\tau^2,\ldots,\tau^{12}$, can be readily obtained using the transformation given by Eq. (4) [30]. The slip plane and slip direction of the 12 primary octahedral slip systems are given in Table 1 [30]

$$\begin{Bmatrix} \tau^1 \\ \tau^2 \\ \tau^3 \\ \tau^4 \\ \tau^5 \\ \tau^6 \\ \tau^7 \\ \tau^8 \\ \tau^9 \\ \tau^{10} \\ \tau^{11} \\ \tau^{12} \end{Bmatrix} = \frac{1}{\sqrt{6}} \begin{bmatrix} 1 & 0 & -1 & 1 & 0 & -1 \\ 0 & -1 & 1 & -1 & 1 & 0 \\ 1 & -1 & 0 & 0 & 1 & -1 \\ -1 & 0 & 1 & 1 & 0 & -1 \\ -1 & 1 & 0 & 0 & -1 & -1 \\ 0 & 1 & -1 & -1 & -1 & 0 \\ 1 & -1 & 0 & 0 & -1 & -1 \\ 0 & 1 & -1 & -1 & 1 & 0 \\ 1 & 0 & -1 & -1 & 0 & -1 \\ 0 & -1 & 1 & -1 & -1 & 0 \\ -1 & 0 & 1 & -1 & 0 & -1 \\ -1 & 1 & 0 & 0 & 1 & -1 \end{bmatrix} \begin{Bmatrix} \sigma_{xx} \\ \sigma_{yy} \\ \sigma_{zz} \\ \sigma_{xy} \\ \sigma_{zx} \\ \sigma_{yz} \end{Bmatrix} \tag{4}$$

Three-Dimensional Elastic Anisotropic FEA of Notched Single Crystal Specimens and Prediction of Slip Sectors

An ideal test would incorporate parameters for specimen size, type of test, plasticity, hardening, lattice rotation, etc., and eventually a fatigue crack rather than a notch. However, before incorporating such complexity the basic model must be better understood. We present a numerical and experimental investigation of 3D stress fields and evolution of slip sector boundaries near notches, using double-notched tensile specimens of a single-crystal superalloy, which has a fcc crystal structure. A 3D linear elastic finite element model that includes the effect of material anisotropy is shown to predict active slip planes and sectors at the specimen surface accurately.

Three-dimensional FEA incorporating elastic anisotropy was used to model test specimens with a fixed [001] primary crystallographic orientation and two different secondary orientations (as shown in Fig. 1) to predict slip activity and sectors around the notch. The two specimens examined have the load direction along the [001] primary orientation, while the notch directions are $[\bar{1}10]$ for specimen A and [010] for specimen B. Three-dimensional FEA of notched single-crystal specimens was accomplished using ANSYS finite element software (Version 5.7). Figure 2 defines the specimen dimensions whose values are given in Table 2. The FEA component stresses were taken from the material coordinate system, around the notch, and then used in the transformation equations to calculate the individual resolved shear stresses. Data were analyzed over a wide range of radial and angular distances to create a complete stress field, and later used to draw conclusions on sectors and slip activation.

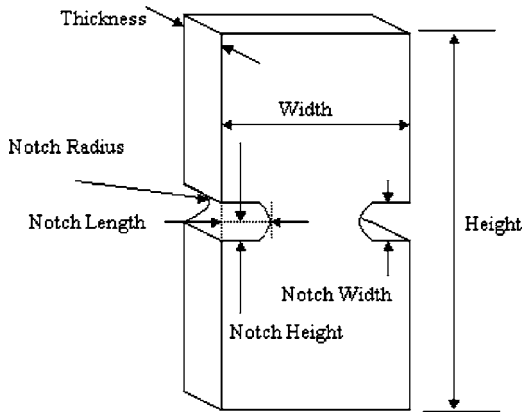

Fig. 2 Dimensions of specimen A [31]

ANSYS aligns material properties with the element coordinate system; therefore, the element coordinate system is aligned with the material coordinate system so that the directional material properties are suitably applied. The ANSYS elements chosen for the FEM are PLANE2 (2D six-node triangular element with quadratic displacement functions) and SOLID95 (3D structural solid with 20 nodes) capable of incorporating anisotropic properties. Figure 3 shows the 3D FE model of specimen A and a close-up view of the notch mesh. After the three-dimensional solid model is created, the front face is meshed with the PLANE2 (two-dimensional) elements. This front face has precise element sizing along the defined radial lines around the notch tip at 5 deg intervals [Fig. 4(*a*)]. Once the front face is meshed, three-dimensional elements are swept through the volume to complete the meshing of the model and the two-dimensional mesh is deleted.

Table 2 Actual and finite element specimen dimensions in mm [31]

Dimensions	Specimen A		Specimen B	
	Actual	FEM	Actual	FEM
Width	5.100	5.100	5.04	5.04
Height	19.000	19.000	17.594	17.594
Thickness	1.800	1.800	1.82	1.82
Right notch length	1.300	1.550	1.399	1.399
Left notch length	1.550	1.550	1.36	1.399
Right notch height	0.113	0.113	0.084	0.084
Left notch height	0.111	0.113	0.0845	0.084

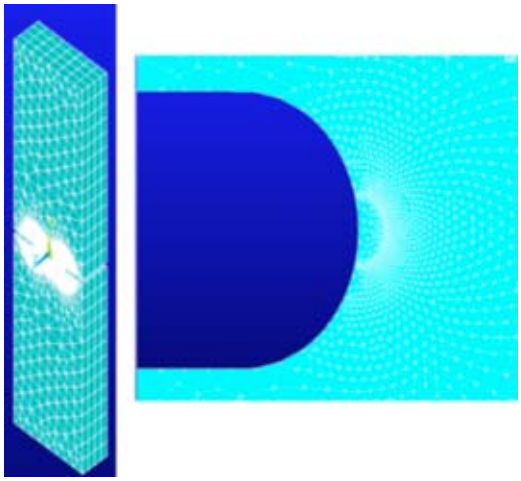

Fig. 3 3D Finite element model of specimen A with a close-up view of the notch [31]

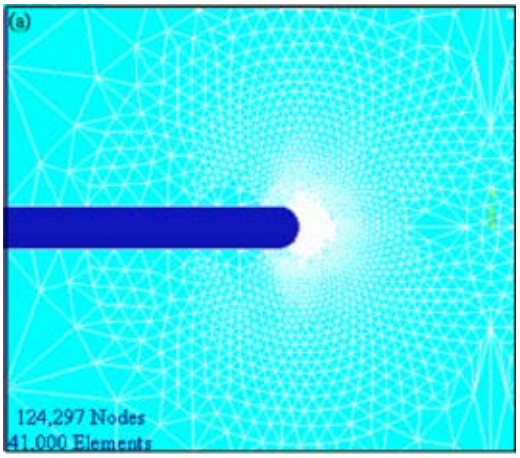

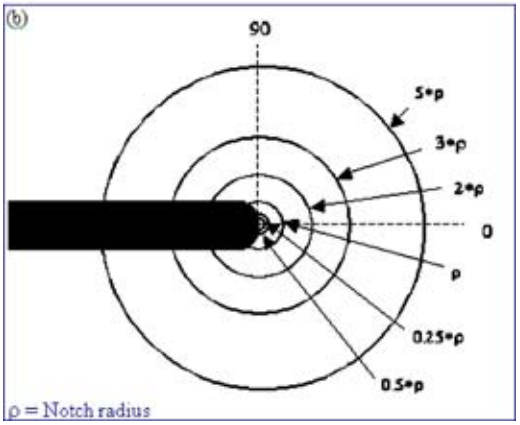

Fig. 4 (*a*) Close-up view of element sizing on the specimen front face near the notch and (*b*) Radial and angular coordinates used for producing slip sector plots [32]

To observe both the near-field and far-field state of stress in the vicinity of the notch (radial and angular), six concentric arcs were created at the following radii from the notch tip: $0.25^*\rho$, $0.50^*\rho$, $1.00^*\rho$, $2.00^*\rho$, $3.00^*\rho$, and $5.00^*\rho$; where ρ is the notch radius [Fig. 4(*b*)]. The element sizing of the FEM allows data to be collected on any of five separate x-y planes, including the front, middle, and back planes.

Results From Finite Element Analysis

Results were plotted for the 12 primary RSS values from $r = 0.25^*\rho$ to $5^*\rho$ and from 0 deg to the top of the notch (100 deg for $0.25^*\rho$ up to 170 deg for $5^*\rho$). Figure 5(a) shows a representative plot of RSS values of 12 primary slip systems, on the surface of specimen A, as a function of theta, at $r = 5\rho$. As a stress-based process, slip deformation can be predicted by the numerical model's highest individual resolved shear stresses. The slip systems that are represented by the highest resolved shear stresses, which exceed the experimentally measured critical resolved shear stress (CRSS) value, should then be observable as slip lines in the experimental test samples. The experimentally determined CRSS value of 47 ksi for the primary slip systems is shown as a dark horizontal line in Fig. 5. The dominant slip systems shown in Fig. 5(*a*) (τ^1 from 0 to 54 deg, τ^2 from 54 to 68 deg, τ^6 from 68 to 86 deg, τ^2 from 86 to 122 deg, and τ^3

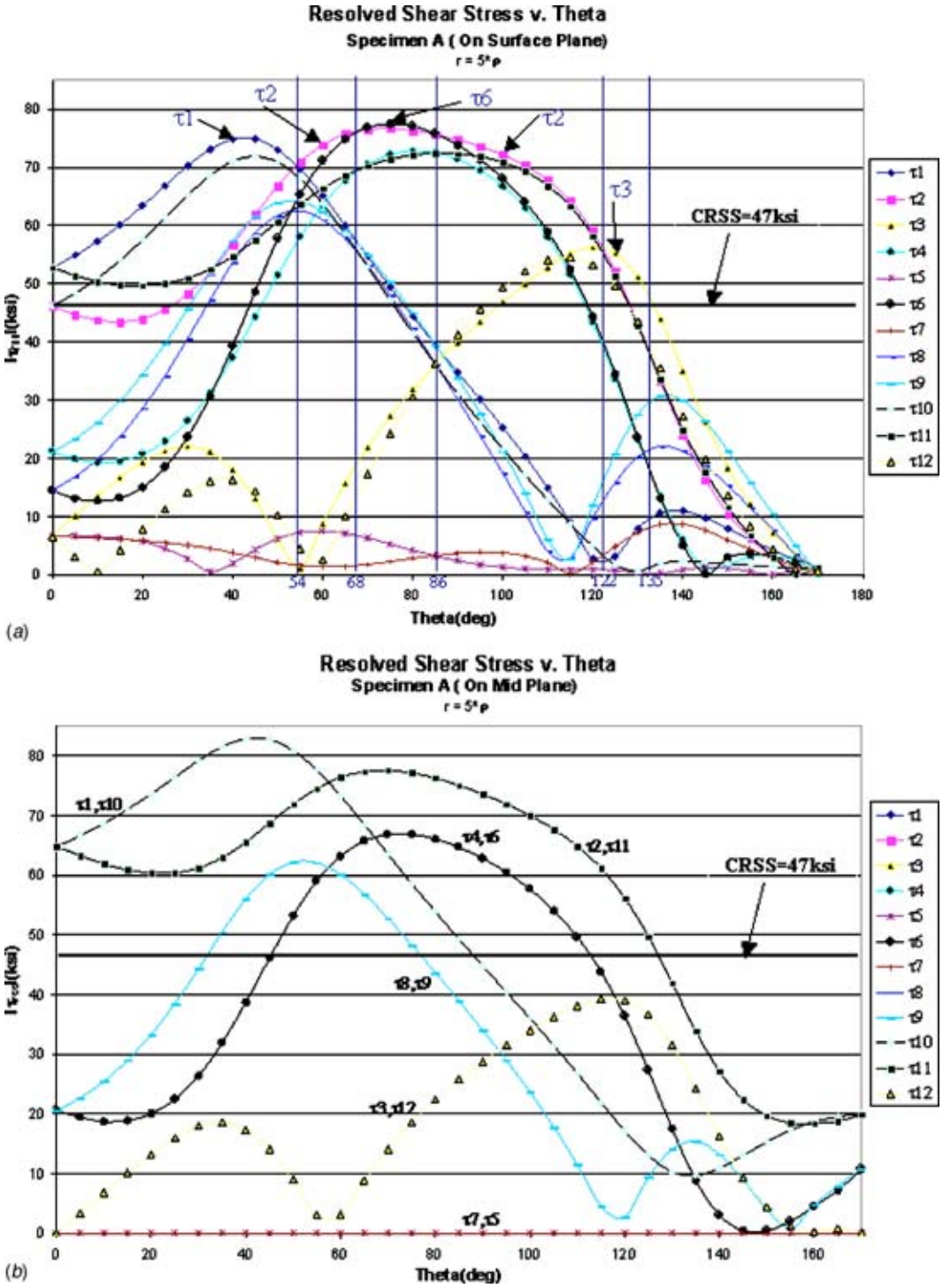

Fig. 5 (*a*) **RSS values (specimen A) for the 12 slip systems, as a function of theta, at $r=5*\rho$ on surface [32]; and (*b*) RSS values (specimen A) for the 12 slip systems, as a function of theta, at $r=5*\rho$ on midplane [32]**

from 122 to 135 deg), with RSS values above 47 ksi will be activated at that radial and angular location. Although there are other slip systems with RSS values above the CRSS value, the only observed slip systems are the dominant ones.

The slip system with the maximum RSS varies with radial and angular position; sectors were determined for each radius by the overall maximum RSS or the dominant slip system. By carefully studying the RSS plots from $r=0.25*\rho$ to $5*\rho$ a comprehensive picture of activated slip systems emerges. Figure 6 shows activated regions with different colors indicating activated slip systems, around the notch, for specimens A, at the surface. For example, at $r=0.25*\rho$, τ^{11} is activated from 0 to 17 deg, and at $r=5*\rho$, τ^{1} is activated from 0 to 54 deg, and so on. Table 4 also summarizes the dominant slip systems at the surface of specimen A, as a function of θ and r.

The RSS values at the midplane were consistently higher than those at the surface, as shown in Fig. 5(*b*). This indicates that slip is likely to initiate at the midplane and progress to the surface. Crone and Shield [23] also note that slip systems may be activated

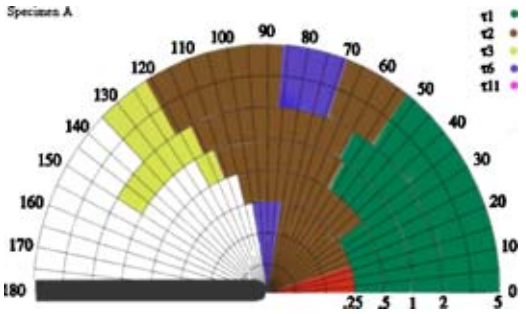

Fig. 6 Dominant and active slip systems at the surface of specimen A as a function of θ and r [32]

internally, rather than at the surface. It is also observed in Fig. 5(*b*) that dominant slip systems occur in pairs (τ^1 and τ^{10}, τ^2 and τ^{11}). The RSS values for other nondominant slip systems also occur in pairs (τ^5 and τ^7, τ^4 and τ^6, τ^3 and τ^{12}, τ^8 and τ^9).

The radial variation produced lobed sectors, rather than straight sectors with constant boundaries (Fig. 6). Note that the boundaries are shaped more like lobes than the constant pie-slice radial boundaries depicted by Rice [16] and Crone and Shield [23].

Comparison of Experimental Results With Finite Element Analysis

Experimental slip field results produced from tensile testing of specimens A and B were compared to FEA predictions. We will discuss the comparison of numerical and experimental results at $r=5*\rho$, as shown in Fig. 7 and summarized in Table 3. The FEA results predict slip activation from 0 to 135 deg; however, in the experimental test, slip activation is only visible at the given radius up to 110 deg.

The exact slip system cannot be determined by the slip trace analysis alone; nonetheless, correlating the known slip plane to the numerical prediction is still a good measure of the model's accuracy. The single dominant slip system plane predicted for each sector by the FEA and those indicated by the experimental specimen match well (Table 3). The crystal orientation of the tested single-crystal specimen A deviated 8 deg from the ⟨001⟩ load direction. This deviation may result in the apparent asymmetry in certain sectors between the positive and negative half

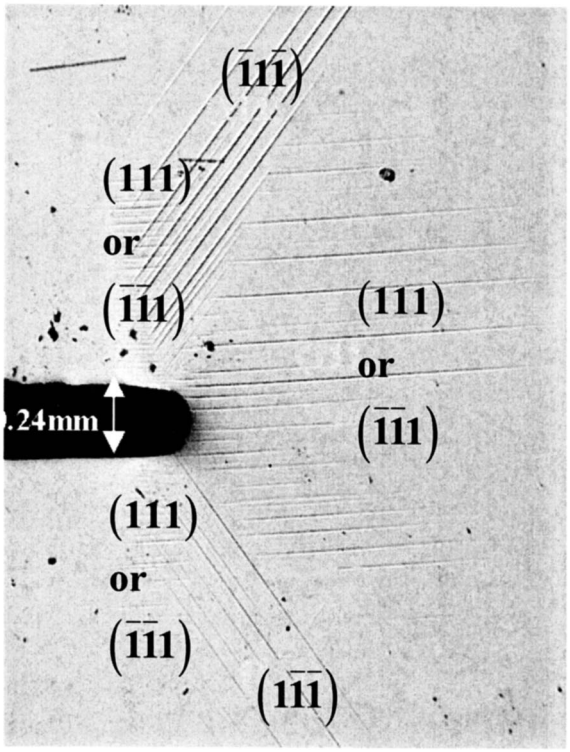

Fig. 7 Experimental slip field results on the surface for specimen A

Table 3 Summary of numerical and experimental results for specimen A at $r=5*\rho$ [31,32]

Dominant Slip System Sectors Specimen A r=5*ρ									
	Numerical solution			Experimental results		Isotropic solution		Rice solution	
Sector	θ	τ max	Slip system	θ	Slip plane	θ	Slip plane	θ	Slip plane
I	0–54	τ_1	(111) [10$\bar{1}$]	0–68	(111) or ($\bar{1}\bar{1}$1)	0–56	(111)	0–55	($\bar{1}$11) and (1$\bar{1}$1)
II	54–68	τ_2	(111) [0$\bar{1}$1]			56–115	(111)	55–90	($\bar{1}$11) and (11$\bar{1}$) or (111)
III	68–86	τ_6	($\bar{1}\bar{1}\bar{1}$) [011]	68–90	($\bar{1}$1$\bar{1}$)	—	—	90–125	(1$\bar{1}$1) and (11$\bar{1}$) or (111)
IV	86–122	τ_2	(111) [0$\bar{1}$1]	85–115	(111) or ($\bar{1}\bar{1}$1)	—	—	125–180	($\bar{1}$11) and (1$\bar{1}$1)
V	122–135	τ_3	(111) [1$\bar{1}$0]	—	—	—	—	—	—

Table 4 Numerical prediction of dominant slip systems on the surface of specimen A, for varying radii *r* from the notch [31,32]

Dominant Slip System Sectors Specimen A									
	r=0.25*ρ			r=0.5*ρ			r=1*ρ		
Sector	θ	τ max	Slip system	θ	τ max	Slip system	θ	τ max	Slip system
I	0–17	τ_{11}	$(\bar{1}\bar{1}1)$ [101]	0–35	τ_1	(111) $[10\bar{1}]$	0–57	τ_1	(111) $[10\bar{1}]$
II	17–82	τ_2	(111) $[0\bar{1}1]$	35–105	τ_2	(111) $[0\bar{1}1]$	57–113	τ_2	(111) $[0\bar{1}1]$
III	82–100	τ_6	$(\bar{1}1\bar{1})$ [011]	⋯	⋯	⋯	113–120	τ_3	(111) $[1\bar{1}0]$

	r=2.0*ρ			r=5.0*ρ		
Sector	θ	τ max	Slip system	θ	τ max	Slip system
I	0–59	τ_1	$(111)[10\bar{1}]$	0–54	τ_1	$(111)[10\bar{1}]$
II	59–116	τ_2	$(111)[0\bar{1}1]$	54–68	τ_2	$(111)[0\bar{1}1]$
III	116–150	τ_3	$(111)[1\bar{1}0]$	68–86	τ_6	$(\bar{1}1\bar{1})[011]$
IV	⋯	⋯	⋯	86–122	τ_2	$(111)[0\bar{1}1]$
V	⋯	⋯	⋯	122–135	τ_3	$(111)[1\bar{1}0]$

planes, as well as any sector boundary differences. Furthermore, the specific irregularities in the notch cutouts may have a different effect from the simplifications of symmetry made in the FEM. The discrepancies seen between the numerical and analytical models may be due to the elastic simplifications of the model, but may also be attributed in part to the 8° deviation from [001] for the experimental load axis.

Specimen B was also analyzed using similar techniques. Figure

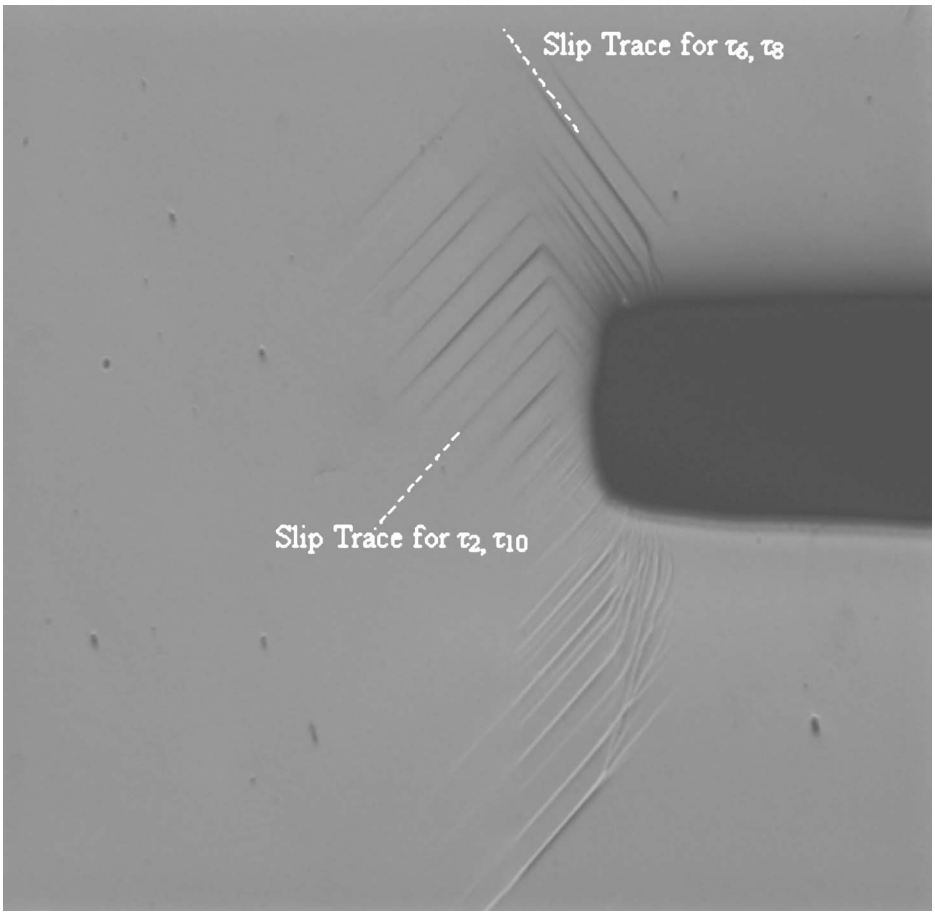

Fig. 8 Experimental slip field results on the surface for specimen B

Table 5 Numerical prediction of dominant slip systems on the surface of specimen B, for varying radii *r* from the notch [32]

Dominant Slip System Sectors Specimen B									
	r=0.25*ρ			r=0.5*ρ			r=1*ρ		
Sector	θ	τmax	Slip system	θ	τmax	Slip system	θ	τmax	Slip system
I	0–41	τ_8	$(1\bar{1}\bar{1})[0\bar{1}1]$	0–56	τ_8	$(1\bar{1}\bar{1})$ $[0\bar{1}1]$	0–52	τ_{10}	$(\bar{1}\bar{1}1)$ $[011]$
II	41–100	τ_6	$(\bar{1}1\bar{1})[011]$	56–105	τ_6	$(\bar{1}1\bar{1})$ $[011]$	52–56	τ_2	(111) $[0\bar{1}1]$
III	…	…	…	…	…	…	56–116	τ_6	$(\bar{1}1\bar{1})$ $[011]$
IV	…	…	…	…	…	…	116–120	τ_4	$(\bar{1}1\bar{1})$ $[10\bar{1}]$

	r=2.0*ρ			r=5.0*ρ		
Sector	θ	τmax	Slip system	θ	τmax	Slip system
I	0–50	τ_{10}	$(\bar{1}\bar{1}1)[011]$	0–46	τ_{10}	$(\bar{1}\bar{1}1)[011]$
II	50–60	τ_2	$(111)[0\bar{1}1]$	46–56	τ_2	$(111)[0\bar{1}1]$
III	60–68	τ_3	$(111)[1\bar{1}0]$	56–64	τ_3	$(111)[1\bar{1}0]$
IV	68–150	τ_6	$(\bar{1}1\bar{1})[011]$	64–131	τ_6	$(\bar{1}1\bar{1})[011]$

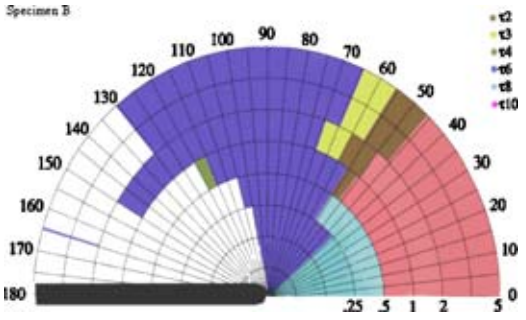

Fig. 9 Dominant and active slip systems at the surface of specimen B as a function of θ and *r* [32]

8 shows the experimentally predicted slip field results, while Table 5 summarizes the numerical results. Numerically predicted slip systems for specimen B agree extremely well with experimental results, as in specimen A. Experimentally observed slip field results are seen to be very different from those of specimen A, highlighting the importance of crystal orientation in activating specific slip systems. Figure 9 shows the dominant slip sector boundaries at the surface of specimen B, as a function of θ and r. Comparison of the results between Figs. 6 and 9 show that the activated slip systems for the two specimen orientations are very different, as is also evidenced by the experimental slip fields. The RSS values at the specimen midplane were also higher for specimen B, and occurred in pairs, indicating again that slip is likely initiated at the midplane first.

Conclusions

A detailed experimental and numerical investigation of 3D stress fields and evolution of slip sector boundaries near notches in fcc single-crystal tension test specimens is presented, as a function of crystallographic orientation. Results demonstrate that a 3D linear elastic finite element model that includes the effect of material anisotropy predicts active slip planes and sectors accurately. The slip sector boundaries are shown to have complex curved shapes with several slip systems active simultaneously near the notch. Slip sectors determined by the stress field are not constant for a given material, as generally indicated by the literature [16,21–23], but are determined by the applied load. Slip sector boundaries on the surface showed excellent agreement with experimental results. Slip systems activated are shown to be a strong function of crystallographic orientation. Results are presented for the surface and midplane of the specimens. The RSS values at the midplane were consistently higher than at the surface, for both orientations examined, indicating that slip might indeed initiate at the midplane and progress to the surface. The results presented demonstrates that accounting for 3D elastic anisotropy is very important for accurate prediction of slip activation near fcc single-crystal notches under a triaxial state of stress. A linear elastic model can be used to predict the initial slip, based on the CRSS value for the slip system, but cannot predict subsequent behavior due to plasticity around the notch tip. Some other modeling assumptions include low temperature deformation, no account of microstructural (i.e., dislocation) mechanisms, and no crystal lattice rotation. However, for this analysis, we have used the FEA results to only predict the onset of yield on slip systems and not the subsequent effects of plasticity. These advanced effects will be included in subsequent modeling efforts currently underway.

Acknowledgments

This work was partially supported by the NASA Marshall Space Flight Center, Huntsville, AL, and Pratt & Whitney, West Palm Beach, FL. The authors would like to thank Dr. Gregory R. Swanson at NASA MSFC, and William Mitchell and Fred Haake at Pratt & Whitney, FL, for the support. The authors would also like to thank Dan Deluca at Pratt & Whitney, East Hartford, CT, for supplying the single-crystal casting from which the tension test specimens were machined.

References

[1] Shrivastava, S., and Ebrahimi, F., 1997, "Effect of Crystallographic Orientation on the Fracture Toughness of NiAl Single Crystals," Mater. Res. Soc. Symp. Proc., **460**, pp. 393–398.
[2] Gumbsch, P., Riedle, J., Hartmaier, A., and Fischmeister, H. F., 1998, "Controlling Factor for the Brittle-to-Ductil Transition in Single Crystals," Science, **282**, pp. 1293–1295.
[3] Ebrahimi, F., and Kalwani, K., 1999, "Fracture Anisotropy in Silicon Single Crystal," Mater. Sci. Eng., A, **268**, pp. 116–126.

[4] Arakere, N. K., and Swanson, G., 2002, "Effect of Crystal Orientation on Fatigue Failure of Single Crystal Nickel Base Turbine Blade Superalloys," ASME J. Eng. Gas Turbines Power, **124**, pp. 161–176.
[5] Swanson, G., and Arakere, N. K., "Fatigue Failure of Single Crystal Nickel Base Turbine Blade Superalloys," NASA/TP-2000-210074.
[6] Arakere, N. K., [YEAR], "High Temperature Fatigue Properties of Single Crystal Superalloys in Air and Hydrogen," *Proc. of ASME Turbo Expo 2000*, June 4–7, New Orleans, ASME, New York, ASME Paper No. 01-GT-585.
[7] Moroso, J., 1999, "Effect of Secondary Orientation on Fatigue Crack Growth in Single Crystal Turbine Blades," M.S. thesis, Mechanical Engineering Department, University of Florida, Gainesville, FL.
[8] Arakere, N. K., and Moroso, J., 2001, "Fatigue Failure in High Temperature Single Crystal Superalloy Turbine Blades," High Temp. Mater. Process., **20**(2), pp. 117–135.
[9] Arakere, N. K., and Swanson, G., 2001, "Analysis of Fretting Stresses in Single Crystal Ni-Base Turbine Blade Attachment Regions," ASME J. Tribol., **123**, pp. 413–423.
[10] Bilby, B. A., Cottrell, A. H., and Swinden, K. H., 1962, "The Spread of Plastic Yield From a Notch," Proc. R. Soc. London, Ser. A, **272**, pp. 304–314.
[11] Rice, J. R., and Thomson, R., 1974, "Ductile Versus Brittle Behavior of Crystals," Philos. Mag., **29**, pp. 73–97.
[12] Kobayashi, S., and Ohr, S. M., 1980, "In-Situ Fracture Experiments in BCC Metals," Prog. Met. Phys., **42**, pp. 763–772.
[13] Majumdar, B. S., and Burns, S. J., 1981, "Crack Tip Shielding—Anelastic Theory of Dislocation and Dislocation Arrays Near a Sharp Crack," Acta Metall., **29**, pp. 579–588.
[14] Weertman, J., Lin, I.-H., and Thomson, R., 1983, "Double Slip Plane Crack Model," Acta Metall., **31**, pp. 473–482.
[15] Gerberich, W. W., Oriani, R. A., Lii, J.-J., Chen, X., and Foecke, T., 1991, "Necessity of Both Plasticity and Brittleness in the Fracture Thresholds of Iron," Philos. Mag., **63**, pp. 363–376.
[16] Rice, J. R., 1987, "Tensile Crack Tip Fields in Elastic-Ideally Plastic Crystals," Mech. Mater., **6**, pp. 317–335.
[17] Rice, J. R., and Saeedvafa, M., 1987, "Crack Tip Singular Fields in Ductile Crystals With Taylor Power-Law Hardening," J. Mech. Phys. Solids, **36**, pp. 189–214.
[18] Saeedvafa, M., and Rice, J. R., 1988, "Crack Tip Singular Fields in Ductile Crystals With Taylor Power-Law Hardening, II: Plane-Strain," J. Mech. Phys. Solids, **37**, pp. 673–691.
[19] Rice, J. R., Hawk, D. E., and Asaro, R. J., 1990, "Crack Tip Fields in Ductile Crystals," Int. J. Fract., **42**, pp. 301–321.
[20] Saeedvafa, M., and Rice, J. R., 1992, "Crack Tip Fields in a Material With Three Independent Slip Systems: NiAl Single Crystal," Modell. Simul. Mater. Sci. Eng., **1**, pp. 53–71.
[21] Shield, T. W., 1996, "Experimental Study of the Plastic Strain Fields Near a Notch Tip in a Copper Single Crystal During Loading," Acta Mater., **44**, pp. 1547–1561.
[22] Schulson, E. M., and Xu, Y., 1997, "Notch-Tip Deformation of Ni_3Al Single Crystals," Mater. Res. Soc. Symp. Proc., **460**, pp. 555–560.
[23] Crone, W., and Shield, T., 2001, "Experimental Study of the Deformation Near a Notch Tip in Copper and Copper-Beryllium Single Crystals," J. Mech. Phys. Solids, **49**, pp. 2819–2838.
[24] Li, X. M., Chiang, F. P., Wu, J., and Dudley, M., 1992, "Experimental Measurement of the Crack Tip Strain Field in a Single Crystals," Eng. Fract. Mech., **43**, 171–184.
[25] Shield, T. W., and Kim, K.-S., 1994, "Experimental Measurement of the Near Tip Strain Field in an Iron-Silicon Single Crystal," J. Mech. Phys. Solids, **42**, 845–873.
[26] Pierce, D., Asaro, R. J., and Needleman, A., 1983, "Material Rate Dependence and Localized Plastic Deformation in Crystalline Solids," Acta Mater., **31**, pp. 1951–1976.
[27] Mohan, R., Ortiz, M., and Shih, C., 1992, "An Analysis of Cracks in Ductile Single Crystals—II. Mode I Loading," J. Mech. Phys. Solids, **40**(2), pp. 315–337.
[28] Cuitino, A., and Ortiz, M., 1996, "Three-Dimensional Crack Tip Fields in Four-Point Bending Copper Single-Crystal Specimens," J. Mech. Phys. Solids, **44**(6), pp. 863–904.
[29] Lekhnitskii, S. G., 1993, *Theory of Elasticity of an Anisotropic Elastic Body*, Holden-Day, San Francisco, pp. 1–40.
[30] Stouffer, D., and Dame, L., 1996, *Inelastic Deformation of Metals: Models, Mechanical Properties, and Metallurgy*, Wiley, New York, pp. 387–417.
[31] Magnan, S., 2002, "Three-Dimensional Stress Fields and Slip Systems in Single Crystal Superalloy Notched Specimens," M.S. thesis, Dept. of Mech. and Aerospace Eng., University of Florida, Gainesville, FL.
[32] Siddiqui, S. A., 2002, "Finite Element Analysis of Single Crystal Superalloy Notched Tensile Specimens," M.S. thesis, Dept. of Mech. and Aerospace Eng., University of Florida, Gainesville, FL.